Heat and mass transfer during a sudden loss of vacuum in a liquid helium cooled tube – Part I: Interpretation of experimental observations

N. Garceau [a,b], S. Bao [a], W. Guo [a,b,*]

[a] *National High Magnetic Field Laboratory, 1800 East Paul Dirac Drive, Tallahassee, FL 32310, USA*
[b] *Mechanical Engineering Department, Florida State University, Tallahassee, FL 32310, USA*

ABSTRACT

Understanding heat and mass transfer processes involved in a sudden catastrophic loss of vacuum is important for many cryogenic systems around the world for cost, damage prevention, and safety reasons. Continuing research in our lab focuses specifically on studying the sudden vacuum break in beam-line tubes of liquid helium cooled superconducting particle accelerators. In our experiments, loss of vacuum is simulated by venting nitrogen gas from a buffer tank to a liquid helium cooled vacuum tube. Previous experiments with normal helium (He I) have revealed that the gas front propagation rate decreases exponentially (Dhuley and Van Sciver, 2016). This slowing down was attributed to the condensation of the nitrogen gas on the tube inner wall, but a quantitative analysis of the gas dynamics and condensation was lacking. In this paper, we extend the previous experimental work by examining the gas propagation in a longer helical tube system cooled by both He I and superfluid helium (He II). We discuss how the cold section of the tube above the liquid helium bath may affect the gas propagation and can lead to an apparently stronger slowing down effect in the He II cooled tube. We also discuss some limitations in the result interpretation in the previous research. A new theoretical model that systematically describes the gas dynamics and condensation is presented. Preliminary simulation results using the model reproduce some key experimental observations well.

© 2018 Elsevier Ltd. All rights reserved.

1. Introduction

Cryogenic systems, such as cryogenic liquid storage vessels, Nuclear Magnetic Resonance systems (NMR), and particle accelerators are especially concerned with loss of insulating vacuum for safety reasons. Vacuum loss in these cryogenic systems causes a large heat load to be applied to the cryogenic liquid. This liquid then boils which can cause a rapid and dangerous buildup of pressure in the liquid cryogen reservoir [1–4].

In particular, particle accelerators are cryogenic systems which are composed of segments called cryomodules. These cryomodules have two vacuum spaces associated with their design and function. The first vacuum space with multi-layer insulation (MLI) provides insulation for a liquid helium (LHe) bath in which a niobium cavity sits. This vacuum space is often, but not always, isolated per cryomodule. Therefore, if the vacuum shield is lost in one module, the other modules' vacuum shields remain unaffected. The second vacuum space is the center of the niobium cavity where the accelerated particles travel. Niobium cavities are interconnected to create a long beam tube path [5–8]. If there is a leak or rupture into this vacuum space, the gas propagating in the beam tube could affect the entire system. Safety concerns and possible damage as a result of vacuum loss have led to multiple failure studies at accelerator labs [9–12].

At room temperature, sudden loss of vacuum has been studied extensively. Air rushes into the system creating a pressure front which can be measured by pressure probes along the length of a pipe. Speed of the gas shock wave propagating in a room temperature pipe is given by the expression $v_o = 2c_o/(\gamma - 1)$, where γ is the ratio of the specific heats and c_o is the speed of sound in the gas [13]. The propagation speed, also called the "escape speed," of air is approximately 1655 m/s. Experimental room temperature measurements agree reasonably well with theoretical calculations when considering sensor orientation and sensitivity [10,11,14].

When trying to understand failure in accelerators, there are additional heat load effects to be considered. The heat load on an accelerator beam tube's internal surface is presumably the result of air molecules colliding with and sticking to the LHe cooled surface. This freezing or condensation process, also called cryopumping, has been researched by many [15–20]. Literature reports

---

* Corresponding author at: Mechanical Engineering Department, Florida State University, Tallahassee, FL 32310, USA.

  E-mail address: wguo@magnet.fsu.edu (W. Guo).

indicate heat load or heat flux due to the incoming gas after vacuum break to be between 3 kW/m^2 and 40 kW/m^2 [4,20–22]. These cryogenic vacuum loss studies typically are done with a system specific cryogenic tank that are short in comparison to a beam tube. Therefore, the propagation of a gas was not considered in these studies.

In order to understand vacuum break process in an accelerator beam-line tube, one has to consider both gas propagation and gas condensation. Experimental observations of vacuum break in previous research revealed that the gas front slows radically when a condensing and freezing gas rushes into a cold vacuum channel like the center vacuum space of a particle accelerator. Prototype testing at European X-ray free-electron laser (XFEL) and Fermi National Accelerator Laboratory recorded speeds on the order of 10 m/s, which are orders of magnitude smaller the experimentally observed speeds at room temperature [22,23].

Early experiments conducted by Dhuley and Van Sciver in our lab confirmed this slowing down effect [24–26]. These experiments were conducted in straight tube immersed in normal helium (He I). Vacuum in this tube was broken and then the arrival times of the gas front were recorded along the tube. There was an observed exponential slowing of the gas front propagation in the experiments. Dhuley and Van Sciver attributed the deceleration to gas condensing and freezing to the walls [24–26]. However, quantitative analysis on how the gas condensation leads to the observed exponential slowing down is not available. Furthermore, particle accelerators commonly use superfluid helium (He II) at temperatures below 2.17 K because of its highly efficient counterflow heat transfer mechanism [27]. For that reason, Dhuley did additional study in He II and reported preliminary results in his dissertation [26]. The results suggest that He II may have a stronger slowing effect than He I but it is in need of a more systematic study.

This paper describes an improved beam tube system that was built to quantitatively understand the gas propagation phenomena in both He I and He II. We present experimental data which shows an apparently stronger slowing down of the gas propagation in the tube cooled by He II. However, a careful analysis of the data suggests that this stronger slowing is, to a large extent, caused by the cold section of the tube above the liquid level. We also discuss some issues with the simple phenomenological model that Dhuley and Van Sciver used. A more complete model which systematically describes gas dynamics and condensation is presented. Preliminary simulation results based on the new model show key features matching experimental observations.

2. Experimental procedure and results

2.1. Experimental procedure

Vacuum break in a particle accelerator is complex due to complicated geometry of the beam tube's niobium cavities and a highly dynamic gas slowing process. The niobium cavities are designed as a series of elliptical shaped cells with short interconnecting center pipes [5–8]. Dhuley and Van Sciver's propagation studies were done with a straight copper tube immersed in LHe as a simplified version of these beam tubes [24]. However, this system was not appropriate to conduct a comparison of He I and He II experiments. In Dhuley and Van Sciver's straight tube system, vacuum pumping on the LHe bath for achieving He II temperature results in a reduced tube length being immersed in LHe. This shortened length was not adequate to determine the attributes of the decelerating gas front.

A new system was designed with a copper helical tube to have a longer section of tube immersed in He II, which allows for better

characterization of the slowing gas front. Fig. 1 shows a simple schematic of the new helical tube system that we have fabricated. Data of Dhuley and Van Sciver's straight tube system and the new helical tube setup are listed in Table 1 for comparison.

Instead of using air which is a mixture of nitrogen, oxygen and other gases, pure nitrogen gas (99.999% pure) contained in a 230-L buffer reservoir was used. This reservoir also provided a means to control gas density and maintain constant (or slowly varying) inlet flow conditions across experiments. In this experiment, the tank pressure was set to 100 kPa. Following Dhuley and Van Sciver's experimental method, vacuum break was simulated by opening a fast action solenoid valve (25 ms opening time). After the valve, flow into the beam tube was choked and regulated by a venturi.

Gas propagation was measured by temperature increase on the surface of the helical copper tube. Previous research showed temperature sensors to be more responsive to the gas front arrival than the pressure sensors [24,28]. Continuing with the use of this method, eight Lake Shore Cernox® thermometers were encapsulated in 2850 FT Stycast® epoxy to provide insulation from the bulk helium. The encapsulated sensors were mounted to the tube on small depressed flat areas. Indium foil and Apiezon® N thermal grease were used between each sensor and the tube surface to reduce the thermal contact resistance. Stainless steel wire twisted around the tube and varnish from Lake Shore were used to hold the sensor firmly in place. The sensors were placed 72 cm apart on the copper coiled tube as indicated in Fig. 1.

Vacuum pressure at the inlet of the helical tube was measured with a cold cathode gauge (range of 10^{-3}–10^{-7} Torr). Buffer tank pressure was measured with a 1000 Torr MKS 626-Baratron® capacitance manometer. A Kulite® XCQ-092 high speed pressure sensor was also placed in the buffer tank for fast pressure drop recording so mass flow rate could be calculated using the method previously detailed by Dhuley and Van Sciver [24]. A second Kulite® sensor was placed just after the venturi to measure gas properties for simulation purposes. Four Data Translation, Inc. DT9824 USB data acquisition modules and National Instruments LabVIEW® were used to record sensor data at a frequency of 4800 Hz. All data acquisition boxes were time referenced with
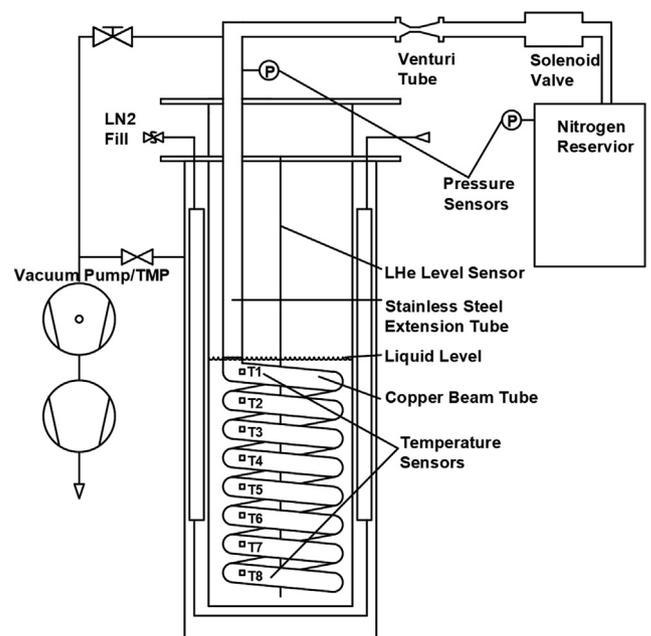

Fig. 1. Schematic of helical tube system.

Table 1
Geometry and setup data of Dhuley and Van Sciver's straight tube system [24] and the new helical tube system.

	Straight	Helical
Copper tube length (m)	1.5	6
Inner tube diameter(mm)	31.1	25.4
Wall thickness (mm)	3	1.25
Coil diameter (mm)	–	229
Coil pitch (mm)	–	50
N_2 reservoir (L)	86	230

the voltage signal to the solenoid valve. This signal was the 'zero time' for all the data recorded for each box.

2.2. He I and He II results

Gas front arrival was determined by a temperature spike on the tube wall after the valve opening. The time of this spike, the rise time t, was recorded to determine the propagation of the gas. To reliably determine the rise time, the sensor data needed to be processed to reduce both random and harmonic noise which varied between data sets. The data for each sensor was smoothed using a 60-point moving average [24]. When the smoothed temperature exceeded a threshold temperature level, the time was noted. This method is similar to the one used in the prior experiments [24]. The He I threshold was set at 0.1 K above the bath temperature which is 4.2 K for LHe at 1 atm. For He II, the threshold was set at 2.17 K, the transition temperature from He II to He I. Fig. 2 shows

the smoothed temperature data with a threshold temperature for both He I (a) and He II (b).

A stronger slowing effect can be observed in the rise times when comparing He I and He II data. For example, rise time for sensor T8 was less than 1400 ms for He I and greater than 2000 ms for He II. Following Dhuley and Van Sciver's method to characterize the deceleration of the gas propagation front in both He I and He II, the rise times obtained from the temperature data were fitted with an exponential function using a non-linear squares regression method [24]:

$$t(x) = a(e^{x/b} - 1) \tag{1}$$

where $t(x)$ is the arrival time at the location x. The liquid level is at $x = 0$. The fitting parameters for the regression are a and b.

The arrival time-location curve can be converted to a velocity equation yielding:

$$v = v_o \cdot e^{-x/b} \tag{2}$$

where $v_o = b/a$ is the entrance velocity [24]. Fig. 3 shows the rise time, $t(x)$, versus the position, x, and the exponential fit of the data. Table 2 shows the calculated values for a, b, and v_o.

These experiments confirm that He II has an apparently stronger slowing effect than He I. The calculated coefficient values as well as the entrance velocities in our experiments are different from those in the Dhuley and Van Sciver experiments [24]. This difference is likely due to geometry and size differences between the two systems. Additionally, in both Dhuley's and the new helical system, the mass flow into the tube is dropping due to decreasing nitrogen reservoir pressure. The helical tube system has a larger buffer reservoir compared to Dhuley and Van Sciver's system which means over the same time interval, there is less change in tank pressure and inlet gas density.

2.3. Effect of condensation point

The presented data show an apparently stronger slowing down effect of gas propagation in the He II experiment. However, we argue that this is not entirely due to the enhanced heat transfer in He II. We note in Table 2 that there appears to be very different entrance velocities in the He I and He II experiments, although both runs are conducted under similar conditions.

An issue not previously considered is the effect of the cold tube section above the liquid surface. If the cold wall is sufficiently low in temperature, the gas can condense on the tube wall. If there is condensation, the conditions or properties of the gas at the start of LHe immersed section, such as density, mass flow rate, etc. will
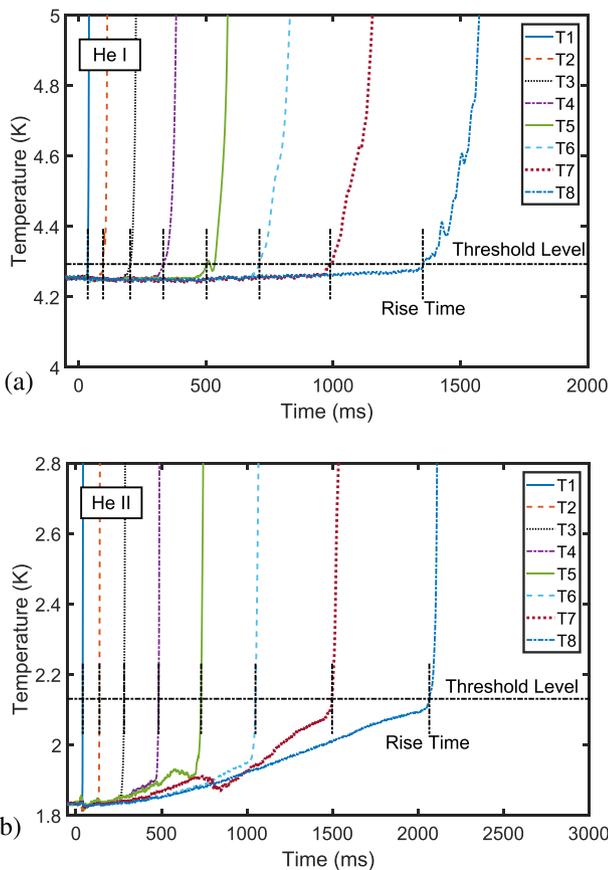

Fig. 2. Smoothed temperature over time data for He I (a) and He II (b) experiments. Threshold level is indicated by a dashed horizontal line. Threshold level is used for determining the rise time of each sensor (short vertical lines).
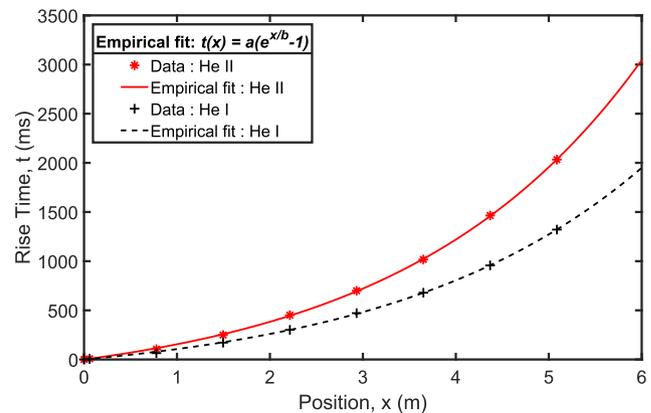

Fig. 3. Graph of the rise time versus the position for both He I and He II experiments.

Table 2
Calculated coefficients and inlet velocity based on actual liquid level at 100 kPa.

	a (s)	b (m)	$v_o = b/a$ (m/s)
Helical tube He I	0.236	2.70	11.42
Helical tube He II	0.323	2.56	7.91
Published He I [24]	0.031	0.63	20.32

Table 3
Calculated coefficients and inlet velocity based on a different condensation point for He II at 100 kPa.

	a (s)	b (m)	$v_o = b/a$ (m/s)
Helical tube He I	0.236	2.70	11.42
Helical tube He II	0.216	2.47	11.4

be different. Tube temperature profile above the liquid was not known and could vary between the runs. This could have led to considerable inconsistency in our data. For instance, the He II experiment requires evaporative cooling by vacuum pumping of the LHe bath. The rush of cold evaporating vapor can cool the upper section of the tube. The temperature profile in this section may strongly depend on the cold vapor flow and hence may vary between runs.

For the data presented in Fig. 2, if we require that the entrance velocities of both He I and He II experiments match, we could shift the assumed condensation point in the He II run by 38 cm above the liquid level. This shift would assume that there is a cold upper section of the tube. After shifting, the exponential fits of the He I and He II experimental data become more closely aligned, as show in Fig. 4. A comparison of the fitting parameters and entrance velocity for He I and the recalculated He II data is shown in Table 3. With the shifted condensation point, the He II data still shows slightly stronger deceleration which is likely due to the larger apparent thermal conductivity of He II [27].

To verify that tube wall was indeed cold enough to condense gas, we measured the temperature profile of the upper portion of the tube. Three sensors were moved higher on the tube. Sensors were placed in 15 cm increments above the coiled tube making the upper most sensor (T1) 12 cm from the top flange. Sensor T4 was located at the beginning of the copper tube and the subsequent sensors (T5–T8) were placed linearly 144 cm apart. New sensor positioning is illustrated in Fig. 5(a).

After moving the sensors, the He II experiment was repeated. Fig. 5(b) shows the temperature profile of the tube during the He II experiment. From the data in Fig. 5(b), it can be seen that some of sensors above the liquid are cold enough to condense gas. The middle sensor, T2, read about 17 K and the lowest sensor, T3, read 3.0 K. Studies of cryopumping indicate that rarefied nitrogen will not stick well to the walls of the tube above 40 K and will stick easily below 20 K [15–20]. Therefore, nitrogen gas should stick to the wall readily in the tube at sensor T2 and below. The observed temperature readings from sensors T2 and T3 show a distinctive sharp rise and flattening like those sensors immersed in the liquid,
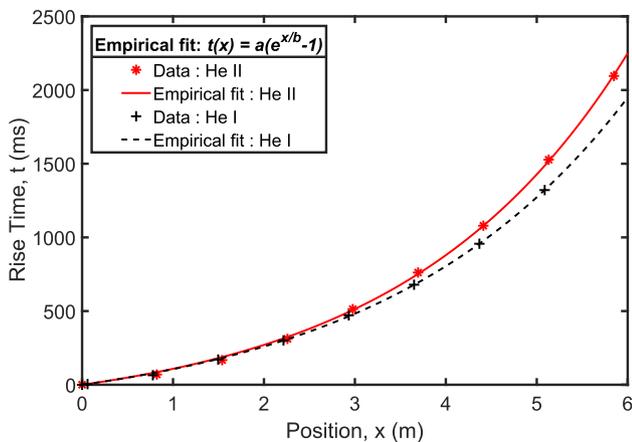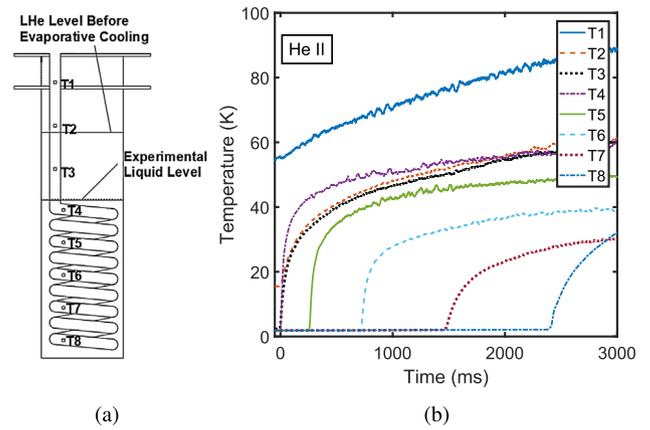

Fig. 5. (a) A simple schematic showing the new positions of the temperature sensors. (b) Temperature data at the new sensor positions during a He II experiment.

which confirms that there is indeed deposition. The actual condensation point should be somewhere between T1 and T2 sensors, which agrees with our assumed condensation point after the 38 cm shift.

3. Theoretical modeling

3.1. Prior conservation of mass model

To explain the observed deceleration of the gas front, Dhuley and Van Sciver proposed a simple model based on conservation of mass analysis in one dimensional tube flow. Expanded explanation and equation derivations can be found in [24,26]. To summarize, as illustrated in Fig. 6, a condensible gas ruptures into a tube with a diameter D at position $X = 0$ (experimentally, $X = 0$ would be the condensation point). The gas flows into the tube at a constant mass flow rate of $\dot{m}_{in}$. After the rupture, at time t, the gas front is located at $X = x$, moving at a speed of $v|_x$. Gas in the region from 0 to x has a density of $\rho(X, t)$ with the density of the gas front being $\rho|_x$. As the gas moves along, it is deposited on the surface of the tube at a rate of $\dot{m}''_{dep}(X, t)$. Based on control mass analysis, a velocity equation can be derived for the gas front [24,26]:

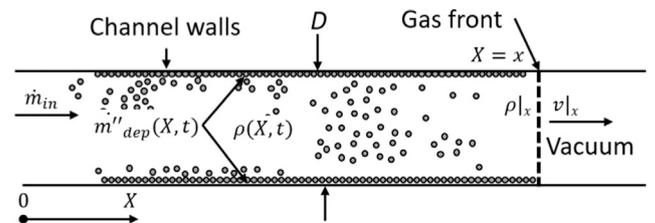$$v|_x = \frac{\dot{m}_{in} - \pi D \int_0^x \dot{m}''_{dep}(X, t)dX}{\frac{\pi D^2}{4} \rho|_x} \tag{3}$$

Fig. 6. Schematic diagram showing the parameters used in the conservation of mass model [24].

Fig. 4. Graph of the rise time versus the position for He I and for He II with the condensation point for He II shifted up by 38 cm.

The slowing down of the gas propagation can be explained using this equation. As time increase, the gas propagates down the tube. The propagation increases the area available for mass deposition which is represented by $\pi D \int_0^x \dot{m}_{dep}''(X,t)dX$ term in Eq. (3). As this mass deposition term increases, the gas front velocity, $v|_x$, decreases.

Although this method captures some aspects of gas slowing down effect, there are some limitations that need to be addressed. First, Dhuley and Van Sciver's proposed model, Eq. (3), explains the slowing of the gas front but it does not give the quantitative exponential deceleration expression as shown by Eq. (2). The second limitation of the model is the arbitrarily defined boundary or propagation front of the control mass analysis. The density of the gas, $\rho|_x$, at the true gas front is essentially zero. This means the calculated velocity, $v|_x$, in Eq. (3) would diverge. If the density is not equal to zero then the velocity is finite and the calculated velocity value will depend on the location of the defined interface. Third, the velocity that was calculated using the rise times of the temperature sensors is not necessarily the velocity given by Eq. (3). The deduced rise time velocity is dependent on the sensitivity of the method with respect to the atoms of gas propagating down the tube. Dhuley showed that temperature sensors were more sensitive to the presence of gas molecules at LHe temperatures than the pressure measurement [28]. Still, the temperature sensors are limited because the temperature rising front is again not the true molecular gas front. Both pressure and temperature sensor cases depend on the density of the gas rising to a point where a signal response can be measured, but this point is not necessarily the same as the control mass boundary or propagation wave front. Finally, $\dot{m}_{in}$ is the mass flow rate calculated based upon changing tank pressure outside the cryostat. However, due to the rapid expansion of the gas into vacuum after the venturi, it is unclear if the mass flow rate and other physical properties are the same at the condensation point as they are immediately after the venturi outside the cryostat. To address the aforementioned limitations with Dhuley and Van Sciver's model, a new theoretical model that systematically incorporates gas propagation and condensation needs to be developed.

3.2. New theoretical model

To properly model the gas propagation in the tube where condensation is a factor, three gas dynamics governing differential equations are needed. The first gas dynamics equation is for the conservation of mass:

$$\frac{\partial \rho}{\partial t} + \frac{\partial}{\partial x}(\rho v) = -\frac{4}{D_1}\dot{m}_c \tag{4}$$

The second gas dynamics equation is the conservation of momentum:

$$\frac{\partial}{\partial t}(\rho v) + \frac{\partial}{\partial x}(\rho v^2) = -\frac{\partial P}{\partial x} - \frac{4}{D_1}\dot{m}_c v \tag{5}$$

The final gas dynamics equation is the conservation of energy:

$$\frac{\partial}{\partial t}\left[\rho\left(\varepsilon + \frac{1}{2}v^2\right)\right] + \frac{\partial}{\partial x}\left[\rho v\left(\varepsilon + \frac{1}{2}v^2 + \frac{P}{\rho}\right)\right]$$
$$= -\frac{4}{D_1}\dot{m}_c\left(\varepsilon + \frac{1}{2}v^2 + \frac{P}{\rho}\right) - \frac{4}{D_1^2}Nu \cdot k(T_g - T_s) \tag{6}$$

Symbol nomenclature for Eqs. (4)–(6) and subsequent equations is provided in Table 4.

Compared to conventional gas dynamic equations, the additional terms on the right hand sides of the above equations are relevant to the mass deposition process on the tube inner wall

Table 4
New theoretical model nomenclature.

Variable	Description
ρ	Gas bulk density
ρ_w	Gas density at the wall surface
v	Gas velocity
P	Gas pressure
T_g	Gas temperature
M	Gas molar mass
$\hat{h}_g$	Gas enthalpy
$\hat{h}_s$	Solid nitrogen enthalpy
ε	Internal energy of the ideal gas
C	Sticking coefficient of gas
R	Ideal gas constant
Nu	Nusselt number
$\dot{m}_c$	Condensation mass flow rate
$\dot{m}_o$	Mass flow rate toward tube wall
x	Position along the tube
D_1	Tube inner diameter
D_2	Tube outer diameter
T_s	Tube wall surface temperature
k	Tube wall thermal conductivity
q	Heat flux into the wall
q_{He}	Heat flux into the helium
C_w	Specific heat of the wall material

surface. We propose the following expression to describe the mass deposition rate, $\dot{m}_c$, due to condensation:

$$\dot{m}_c = \dot{m}_o \cdot C(T_g, T_s, P) = \sqrt{\frac{RT_g}{2\pi M}}\rho \cdot C(T_g, T_s, P) \tag{7}$$

where $\dot{m}_o$ is the mass flow rate toward the tube wall due to thermal motion of the gas molecules for an ideal gas at temperature T_g. We include a sticking coefficient, C, to describe the condensation probability per collision for the gas molecules. The sticking coefficient is a function of both the gas and the wall surface temperatures. Researchers have studied this function for various gases in the free molecular flow region and found that when the gas temperature is relatively low, the sticking coefficient is essentially controlled by the wall temperature [18,19]. The variation of C in continuum flow region is more complex and is still a subject of active research. To illustrate the usefulness of the new model, we adopted a simple profile for the sticking coefficient in our preliminary simulation to be presented in the next subsection. The sticking coefficient of nitrogen is set to 0.6 at low temperatures and smoothly drops to zero as the temperature increases toward the condensation temperature that corresponds to local gas pressure. For instance, Fig. 7 shows an example of the sticking coefficient profile at a location where the gas pressure equals the triple point pressure of nitrogen
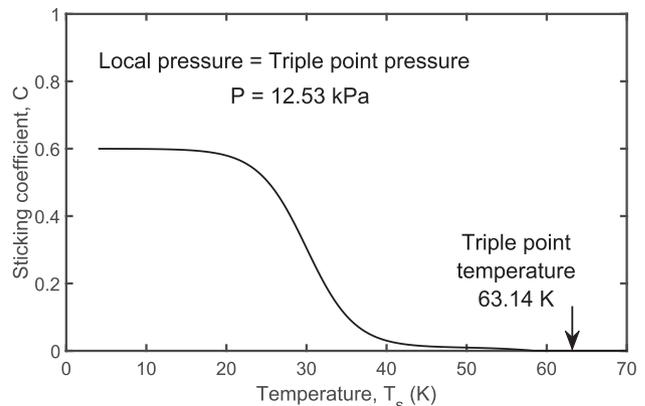

Fig. 7. An example graph of nitrogen's sticking coefficient used in the preliminary simulation for a local gas pressure that equals the triple point pressure.

(i.e., 12.53 kPa [29]). In the future, we plan to allow the sticking coefficient profile to vary such that an optimum simulation result and the experimental observations can be achieved. This procedure should allow us to determine the sticking coefficient in our continuum flow experiments, which will be valuable information for the engineering community.

The temperature of the tube wall is also needed in the model. This temperature can be determined by solving the radial heat transfer equation:

$$\rho_w C_w \frac{D_2^2 - D_1^2}{4D_1} \frac{\partial T_s}{\partial t} = q - q_{He} \frac{D_2}{D_1} \tag{8}$$

This equation has been adopted by Dhuley and Van Sciver [25,26] and it neglects the effect of the building nitrogen frost layer on the surface of the tube. In Eq. (8), q_{He} is the heat flux into the helium which can be evaluated based on published empirical heat transfer models for convective heat transfer, nucleate boiling, and film boiling in a saturated helium bath [27,30]. Heat flux into the wall, q in Eq. (8), is due to both gas convection and gas condensation:

$$q = \dot{m}_c \left[\frac{1}{2} v^2 + \hat{h}_g(T_g, P) - \hat{h}_s(T_s, P) \right] + \frac{Nu \cdot k}{D_1}(T_g - T_s) \tag{9}$$

Furthermore, since the compressibility of the nitrogen gas in our entire experiment is always close to unity, its state can be well described by the ideal gas equation of state:

$$PM = \rho R T_g \tag{10}$$

To determine how gas propagates in the tube where condensation is important, Eqs. (4)–(10) need to be solved simultaneously.

3.3. Preliminary results

We conduct preliminary calculations using the new model. Fig. 8 shows a simple diagram of the tube system used in our simulation. A copper tube with a length of 7 m, inner diameter of 25.4 mm, and a thickness of 1.25 mm is used to match the experimental tube geometry. The tube is assumed to be initially evacuated to a pressure of 10^{-6} Pa. The condensible ideal gas, nitrogen, at 298 K flows into the system at a mass flow rate of 18.3 g/s that matches the experimental mass flow rate determined based on the observed pressure drop in the buffer reservoir [24,26]. Temperature of the first meter of the entrance is set at room temperature. The next 6 m is set to an initial temperature of 4.2 K which simulates a He I bath cooled wall or it is set to a fixed temperature of 160 K for a non-condensing simulation. With the aforementioned boundary conditions, Eqs. (4)–(10) were discretized through the finite difference method based on Godunov's two-step scheme [31], and solved simultaneously in Python.

Fig. 9 shows a comparison of gas density profiles in the 160 K fixed wall temperature simulation and the simulation with He I-cooled tube walls at various propagation times. At time $t = 1$ ms, in both simulations, the bulk part of gas has traveled to approximately the 1 m location and by $t = 81$ ms the gas has saturated in density in the first meter. This clarifies a previous concern about mass flow into the non-condensing region of the tube. By 81 ms,
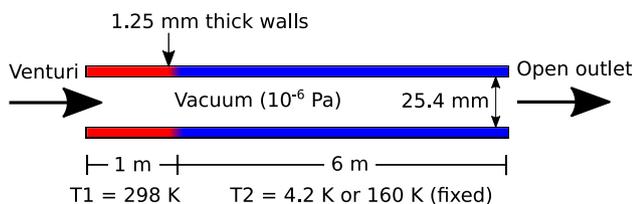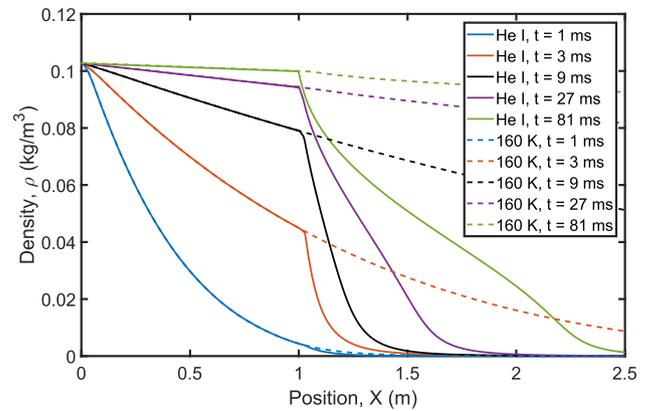

Fig. 9. Simulation comparing densities of condensing (solid lines) and non-condensing (dashed lines) tube walls as a function of time and position.

the mass flow rate and other physical properties of the gas in the non-condensing region have restored to the values measured at the room temperature inlet. This simulation also illustrates what is happening to the gas density in the section after the 1-m warm entrance. There is a sudden decrease in gas density as the gas starts freezing to the walls of the beam tube. This density decrease shows radically slowing gas propagation. For instance at $t = 3$ ms in the He I condensing case, the gas has not reached the 1.75 m location, but in the non-condensing 160 K simulation, the gas front is well past the 2 m location.

For the He I case, the wall temperature is also calculated and is presented in Fig. 10. Comparing the temperature profiles of Fig. 10 to the experimental temperature data of Fig. 5(b), it can be seen that behavior of the sensors immersed in LHe, T4–T8, are similar to the simulated temperatures of the model where position $x = 1.24$ corresponds roughly to sensor T4 and $x = 6.24$ to sensor T8. The model captures how the temperature profiles spike then saturate at a specific temperature after the front passes. It also captures how each saturation temperature at the sensor location is lower than the previous sensor and the temperature spikes become less steep. This behavior is the result of decreasing gas density and velocity down the tube. This simulation starts to resolve the issue of sensor response that is not corrected for in the prior phenomenological model by allowing direct comparison of experimental temperature data to the simplified temperature data. These preliminary results prove that our numerical model has already captured the main physics in the gas propagation along a liquid helium cooled tube, and gives a good reference for the interpretation of experimental results.
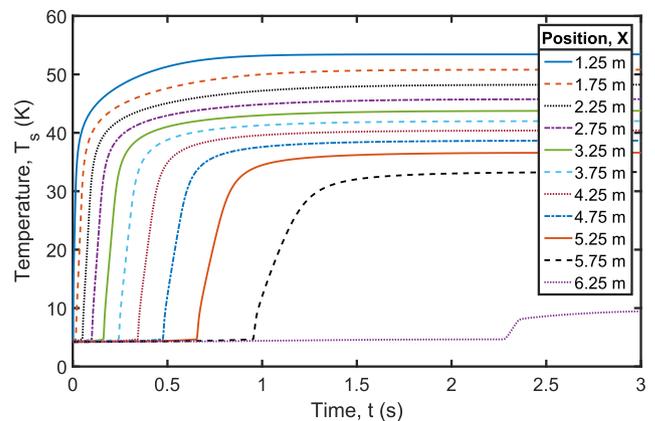

Fig. 8. Schematic diagram showing the tube geometry and initial conditions used in our preliminary simulation.

Fig. 10. Simulated temperature profiles at a fixed location showing propagation slowing as a function of time.

Note that the exact values of rise times and temperature in this preliminary simulation differ from the measured values. This is likely is due to the simplification of the sticking coefficient profile and other factors. For instance, the current model does not take into account the conduction resistance from the nitrogen frost layer deposited on the wall. Furthermore, in the experiment, the non-condensing section is not a constant room temperature segment and the condensing region also varies in temperature down to the LHe bath. In future work, we will take into account all these factors in the model so that accurate quantitative comparison between the experimental measurements and model simulation can be made.

4. Conclusion

This paper describes continuing research in our lab which simulates the sudden vacuum break in beam-line tubes of liquid helium cooled particle accelerators. A new helical beam tube system was fabricated to analyze the slowing effect in both He I and He II experiments. From experimentation and additional analysis, we revealed how the cold section of the tube above the LHe may affect the gas propagation, leading to an apparently stronger deceleration in He II cooled tube. Some limitations of the prior conservation of mass model are discussed. A new model that systematically describes the gas dynamics and condensation of the propagation deceleration phenomena is presented. Preliminary simulation results reproduce several key features seen in the experimental data, which validates the applicability of the new model.

In the future, we plan to advance the model by including other factors that have been neglected in the preliminary simulation. Experimentally, to better compare He I and He II data, the tube system will be modified so its upper section will be thermally insulated such that condensation in the section above the LHe can be avoided. Additionally, it is planned to look at the effect of different mass flow rates as well as different tube geometries and compare the results with a refined model simulation.

Conflict of interest

The authors declared that there is no conflict of interest.

Acknowledgments

References

[1] T.M. Flynn, Cryogenic Engineering: Second Edition Revised and Expanded, CRC Press, Boca Raton, Florida, 2005.

[2] G. Petitpas, S.M. Aceves, Modeling of sudden hydrogen expansion from cryogenic pressure vessel failure. I., J. Hydrogen Energy 38 (2013) 8190–8198, https://doi.org/10.1016/j.ijhydene.2012.03.166.

[3] G.F. Xie, X.D. Li, R.S. Wang, Study on the heat transfer of high-vacuum-multilayer-insulation after sudden, catastrophic loss of insulating vacuum, Cryogenics V50 (2010) 682–687, https://doi.org/10.1016/j.cryogenics.2010.06.020.

[4] S.M. Harrison, Loss of vacuum experiments on a superfluid helium vessel, IEEE Trans. Appl. Supercond. 12-1 (2002) 1343–1346, https://doi.org/10.1109/TASC.2002.1018651.

[5] H. Padamsee, Design Topics for Super Conducting RF Cavities and Ancillaries, Cornell University, CLASSEE, New York, 2018 (accessed May 2018) <https://arxiv.org/ftp/arxiv/papers/1501/1501.07129.pdf>.

[6] Fermilab, Cryomodule design, Fermilab. <https://ilc.fnal.gov/accelerators/cryomodule.html> (accessed April 2018).

[7] T. Khabiboulline, Engineering for Particle Accelerators, Fermilab, 2017. <http://uspas.fnal.gov/materials/17NIU/SRF%20Cavity.pdf> (accessed May 2018).

[8] T. Peterson, Cryogenic conderations for cryomodule design, Fermilab SLAC 2017. <http://uspas.fnal.gov/materials/17UCDavis/Cryogenics/8-Cryomodule%20Design.pptx> (accessed May 2018).

[9] M. Wiseman, K. Crawford, M. Drury, K. Jordan, J. Preble, Q. Saulter, W. Schneider, Loss of cavity vacuum experiment at CEBAF, Adv. Cryogen. Eng. 39 (1994) 997–1003, https://doi.org/10.1007/978-1-4615-2522-6_121.

[10] M. Ady, M. Hermann, R. Kersevan, G. Vandoni, D. Ziemianski, Leak propagation dynamics for the HIE-ISOLDE super conducting LINAC, in: 5th Int. Particle Accelerator Conf. Proc., 2014, pp. 2351–2353. https://doi.org/10.18429/JACoW-IPAC2014-WEPME039.

[11] M. Ady, G. Vandoni, M. Guinchard, P. Grosclaude, R. Kersevan, R. Levallois, M. Faye, Measurement campaign of 21-25 July 2014 for evaluation of HIE-ISOLDE inrush protection system, (Technical Report) Retrieved from CERN Database, (EDMS No. 1414574), 2014.

[12] M. Seidel, D. Trines, K. Zapfe, Failure Analysis of the Beam Vacuum in the Superconducting Cavities of the TESLA Main Linear Accelerator, TESLA-Report 2002-06.

[13] A.H. Shapiro, The Dynamics and Thermodynamics of Compressible Fluid Flow, first ed., vol. 2, The Ronald Press, New York, 1954, pp. 954–947.

[14] T. Takiya, F. Higashino, Y. Terada, A. Koumura, Pressure wave propagation by gas expansion in a high vacuum tube, J. Vac. Sci. Technol. A 17 (4) (1999) 2059–2063, https://doi.org/10.1116/1.58172.

[15] R.F. Brown, D.M. Trayer, M.R. Busby, Condensation of 300-2500 K gases on surfaces at cryogenic temperatures, J. Vac. Sci. Technol. 7-1 (1970) 241–246, https://doi.org/10.1116/1.1315808.

[16] C. Tantos, S. Naris, D. Valougeoris, Gas flow toward an absorbing planar wall subject to partial gas-surface thermal accommodation, Vacuum 125 (2016) 65–74, https://doi.org/10.1016/j.vacuum.2015.12.002.

[17] K.W. Rogers, Experimental investigations of solid nitrogen formed by cryopumping, (Technical contractor report) Retrieved from National Aeronautics and Space Administration, Technical Reports Server, (Report No. NASA-CR-553), 1966.

[18] J. Dawson, J. Haygood, Cryopumping, Cryogenics V5 (2) (1965) 57–67, https://doi.org/10.1016/S0011-2275(65)80002-9.

[19] K.M. Welch, Capture Pumping Technology, second ed., Elsevier Science B.V., Amsterdam, Neatherlands, 2001, https://doi.org/10.1016/B978-0-444-50882-9.X5020-8.

[20] E. Bosque, Transient heat transfer to helium II due to a sudden loss of insulating vacuum, (Dissertation) Retrieved from Florida State University, Proquest Dissertations Publishing database (UMI No. 3625730), 2014.

[21] C. Heidt, S. Grohmann, Modeling the pressure increase in liquid helium cryostats after failure of the insulating vacuum, in: Adv. Cryogen. Eng.: Trans. Cryogen. Eng. Conf., 1573, AIP Publishing, 2014, pp. 1574–1580, https://doi.org/10.1063/1.4860894.

[22] T. Boeckmann, D. Hoppe, K. Jensch, R. Lange, W. Maschmann, B. Petersen, T. Schnautz, Experimental tests of fault conditions during the cryogenic operation of a XFEL prototype cryomodule, in: Proc. of the Int. Cryogenic Engineering Conf. 22 - Int. Cryogenic Materials Conference-2008, Seoul, 2009, pp. 723–728.

[23] A.A. Dalesandro, R.C. Dhuley, J.C. Theilacker, S.W. Van Sciver, Results from sudden loss of vacuum on scaled superconducting radio frequency cryomodule experiment, in: AIP Conf. Proc. 1573, 2014, pp. 1822–1828. https://doi.org/10.1063/1.4860929.

[24] R.C. Dhuley, S.W. Van Sciver, Propgation of nitrogen gas in a liquid helium cooled vacuum tube following sudden vacuum loss - Part I: Experimental investigations and analytical modeling, Int. J. Heat Mass Transfer 96 (2016) 573–581, https://doi.org/10.1016/j.ijheatmasstransfer.2016.01.077.

[25] R.C. Dhuley, S.W. Van Sciver, Propagation of nitrogen gas in a liquid helium cooled vacuum tube following sudden vacuum loss - Part II: analysis of propagation speed, Int. J. Heat Mass Transfer 98 (2016) 728–737, https://doi.org/10.1016/j.ijheatmasstransfer.2016.03.077.

[26] R.C. Dhuley, Gas propagation in a liquid helium cooled vacuum tube following a sudden vacuum loss (Dissertation) Retrieved from Florida State University, Proquest Dissertations Publishing database (UMI No. 10120583), 2016.

[27] S.W. Van Sciver, Helium Cryogenics, second ed., Springer Science+Business Media LLC New York, 2012.

[28] R.C. Dhuley, S.W. Van Sciver, Epoxy encapsulation of Cernox^{TM} SD thermometer for measuring the temperature of surfaces in liquid helium, Cryogenics V77 (2016) 49–52, https://doi.org/10.1016/j.cryogenics.2016.05.001.

[29] National Institute of Standards and Technology, Thermodynamics Source Database: Nitrogen in NIST Chemistry WebBook, SRD 69, National Institute of Standards and Technology, Gaithersburg MD, Web accessed July 2018 URL <https://webbook.nist.gov/cgi/inchi/InChI%3D1S/N2/c1-2>.

[30] W. Steward, Transient helium heat transfer phase I – static coolant, Int. J. Heat Mass Transfer 21 (7) (1978) 863–874, https://doi.org/10.1016/0017-9310(78)90178-3.

[31] G.A. Sod, A survey of several finite difference methods for systems of nonlinear hyperbolic conservation laws, J. Coputational Phys. 27 (1978) 1–31, https://doi.org/10.1016/0021-9991(78)90023-2.